Matter

CellPress

Article

# Investigating the autocatalytically driven formation of Keggin-based polyoxometalate clusters

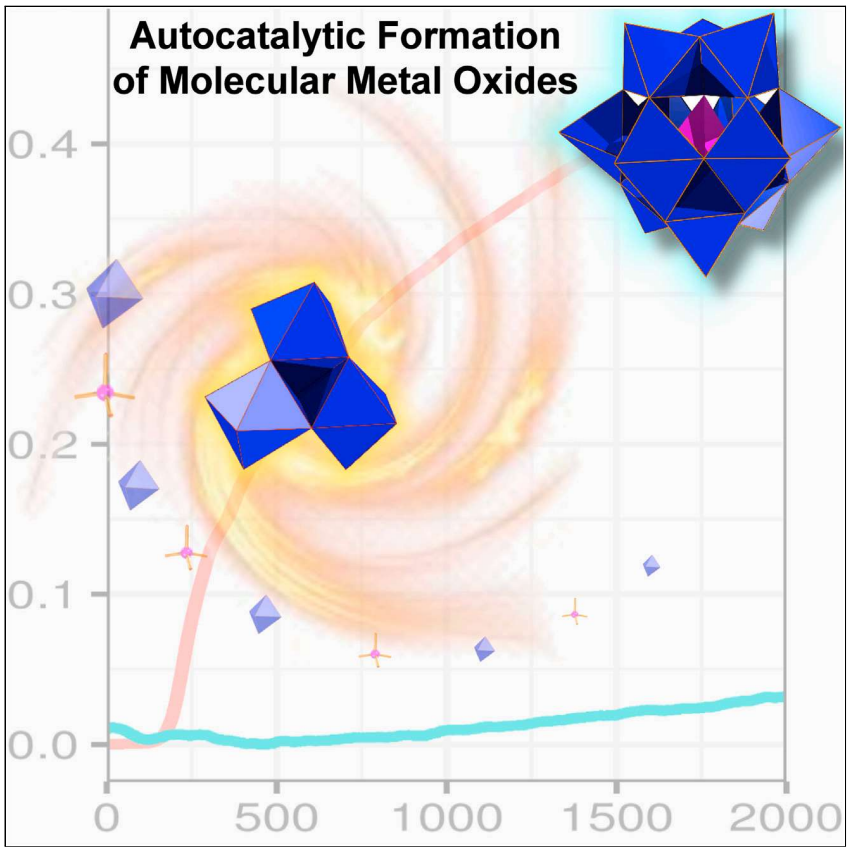


The self-assembly of complex molecular nanostructures using templates that can catalyze their own formation, i.e., undergo autocatalysis, is explored based on the formation of polyoxometalates in solution. The kinetic study confirms that the classic tetrahedral Keggin ion can self replicate, and the role of the central heteroanion is explored with kinetic measurements and stochastic simulations. This approach offers a new route to design complex nanostructures using self-replication and templating as a way of propagating architectural information.

David Lockey, Cole Mathis, Haralampos N. Miras, Leroy Cronin

charalampos.moiras@glasgow.ac.uk (H.N.M.)
lee.cronin@glasgow.ac.uk (L.C.)

## Highlights

Identification of the general self-assembly mechanism of molecular metal oxides

The Keggin ion can catalyze its own formation via an autocatalytic cycle

Identification of the template's effect on the system's autocatalytic traits

Development of a stochastic model that describes the experimental observations


**Understanding**
Dependency and conditional studies on material behavior

Lockey et al., Matter 5, 302–313
January 5, 2022 
https://doi.org/10.1016/j.matt.2021.11.030

CellPress

Matter

Article

# Investigating the autocatalytically driven formation of Keggin-based polyoxometalate clusters

David Lockey,[1] Cole Mathis,[1] Haralampos N. Miras,[1,*] and Leroy Cronin[1,2,*]

## SUMMARY

**The term self-assembly is used to describe the formation of many molecules and supramolecular architectures, but often, the precise mechanism is neglected. Here, we have investigated the kinetics of the self-assembly of the simplest heteropolyoxoanion, the Keggin ion $[XMo_{12}O_{40}]^{x-}$. This study used variable temperature UV/vis spectroscopy to show that the Keggin ion can catalyze its own formation via an autocatalytic cycle. Kinetic investigations with real-time monitoring of the $[XMo_{12}O_{40}]^{x-}$ family's formation reaction revealed key traits of autocatalytic systems, including kinetic saturation and concentration dependence of the incubation period. We explored the effect of the heteroatom on the kinetics of the autocatalytic process by investigating and comparing the formation rates of $\{AsMo_{12}\}$ and $\{SiMo_{12}\}$. Finally, real-time electrospray ionization mass spectrometry studies of the reaction mixtures assist in the identification of the species involved in the formation process of the Keggin species, and these were explored using a stochastic model, which confirms our experimental observations.**

## Progress and potential

As chemistry and materials synthesis embrace the need for discovery of fundamentally new types of chemistry to solve hard problems, it is becoming vital that the understanding and systematic control of real mechanisms masked by complex chemical processes can pave the way to new types of materials discoveries, synthesis, and manufacturing.

## INTRODUCTION

Polyoxometalates (POMs) have been widely studied, largely because they cover a vast range of shapes, sizes, and properties.[1–4] One of the fundamental aspects of POMs is their ability to self-assemble into discrete molecular structures, despite the presence of building block libraries that could combinatorially form an infinite number of alternative structures. These discrete structures range from small clusters such as the $\{Mo_8\}$ (0.7 nm), the $\{Mo_{12}\}$ Keggin (1.0 nm), and the $\{Mo_{36}\}$ (2.1 nm), all the way up to the high nuclearity nanosized species of $\{Mo_{132}\}$ keplerate (2.9 nm), $\{Mo_{154}\}$ (3.6 nm) molybdenum blue wheel, and the protein sized, and largest of all POMs, $\{Mo_{368}\}$ (5.5 nm). Although the process of self-assembly still is not fully understood, recent studies have shown that both the $\{Mo_{36}\}$ and the $\{PMo_{12}\}$ Keggin are involved in the assembly of larger POM structures via a template-mediated process as part of a set of autocatalytic reactions, but it is not known how the smaller clusters form (Figure 1).[5] This is important; the Keggin species is the oldest known POM archetype and was first discovered in 1826.[6] However, it was not until more than a century later that its structure was determined by X-ray crystallography in 1933[7] and it is now, after almost another century has passed, that the intrinsic formation mechanism is being investigated. The lack of earlier mechanistic insights did not prevent the investigation of its chemical reactivity along with other heteropolyanions, which are by far the most explored subset of the POM family.[8–12] These can be described as metal oxide clusters that incorporate heteroatoms such as $PO_4^{3-}$ and $SO_4^{2-}$.[13]

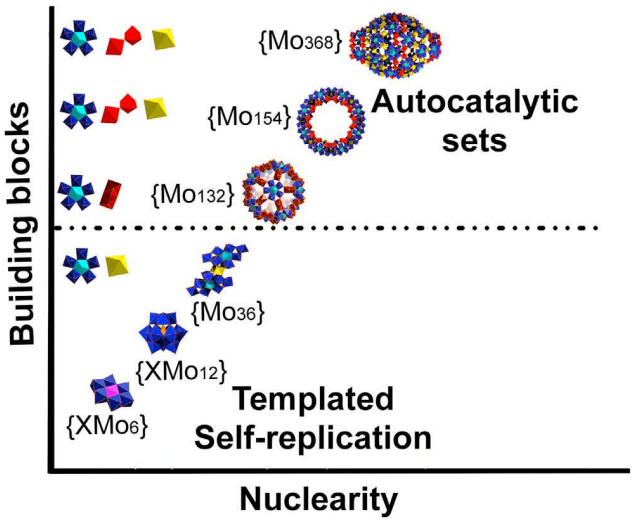


**Figure 1. Polyhedral representation of the fundamental building units involved in the formation of polyoxoanions and size-dependent mechanistic effects that govern their formation**

Investigations into the self-assembly and dynamics of these POM systems has often involved the use of high-resolution mass spectrometry, specifically electrospray (ESI-MS) and cryospray (CSI-MS), as these ionization techniques are mild enough to prevent undesirable fragmentations and allow well-defined identification of structurally related species within the reaction systems. These studies, along with theoretical studies, have allowed us to gain insight into how these complex systems fundamentally behave and how the identified clusters isomerize, speciate, and reassemble.[14–21] Decades of extensive investigations on POMs accompanied by detailed structural characterizations has allowed the discovery of numerous species. The breakdown into various subgroups, such as iso-/hetero-polyanions and molybdenum blues/browns, and the identification of fundamental virtual building blocks, has been essential for the deeper understanding POMs chemical reactivity.

Although extensive studies have probed the self-assembly at the conceptual level or theoretical studies have characterized the bonding invovled,[22–25] it has been difficult to devise a mechanistic and experimental paradigm to investigate the mechanism of the formation. Previously it has been shown that the large POMs just as the {$Mo_{154}$} wheel and {$Mo_{132}$} ball-shaped clusters are formed by a network[5] of mutually catalytic reactions—a so-called autocatalytic set[26–28]—and this explains why these clusters are even possible, and represent magic numbers of stable compounds from the infinite number conceivable. This is important since it hints at the first example of the transfer of templated-based information at the molecular level in an inorganic system outside of biological ones.[29,30] Thus, this work is part of our extended exploration effort, which is based on the hypothesis that the formation of smaller POM-based species involves template-driven autocatalytic cycles, which controls further combinatorial explosion in the reaction mixture making possible the formation of nanosized molecular constituents via cross-catalyzed processes (Figure 1).[5]

Autocatalytic processes are reactions in which a product of the reaction acts as a catalyst for its own formation. One of the characteristic traits of template autocatalytic systems[31–34] is the existence of an induction period, followed by an exponential rise in rate.[35] More specifically, a marked increase of the reaction rate takes place as a function of time, followed by a considerable decrease upon the formation of a

[1]University of Glasgow, Joseph Black Building, University Avenue, Glasgow G12 8QQ, UK
[2]Lead contact
*Correspondence: charalampos.moiras@glasgow.ac.uk (H.N.M.), lee.cronin@glasgow.ac.uk (L.C.)
https://doi.org/10.1016/j.matt.2021.11.030

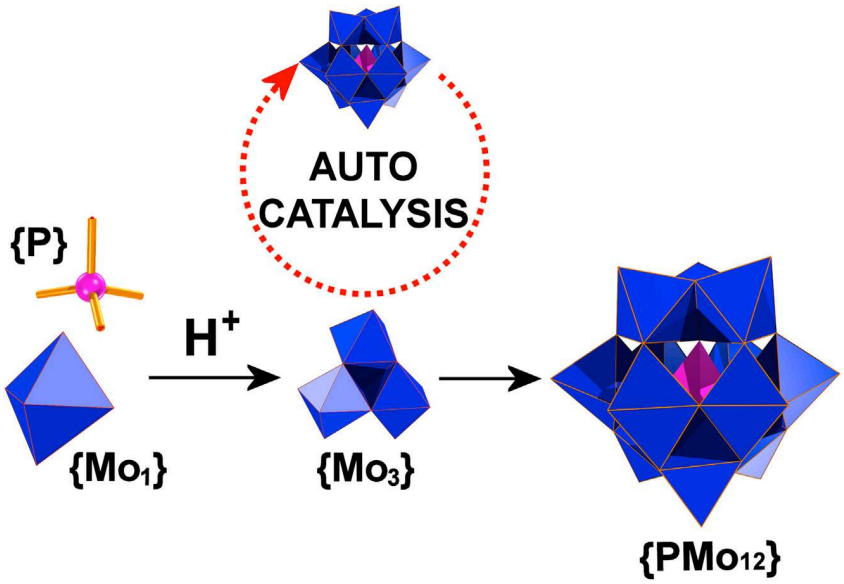


**Figure 2. Formation of $\{PMo_{12}\}$ Keggin species via a $\{PMo_3\}$ templated autocatalytic cycle**

substantial amount of product. This decrease is caused by a combination of two factors—the depletion of the reactants and, in the case that the templating step requires more than one reactant, the number of templates can exceed the number of reactants—meaning that multiple reactants are unlikely to react with a single template, known as kinetic saturation. The use of the term autocatalytic is appropriate only for chemical systems considered under constant temperature and pressure. Crucially, the identification of autocatalytic and self-replication effects does not depend only on the detection of an induction period, but rather on a collection of signatures associated with this process, such as exponential (sigmoidal) product versus time curve with induction period, rate increase, and elimination of the induction period upon seeding of the reaction mixture with preformed product followed by kinetic saturation of the system and deceleration of the species' formation.

In this work we hypothesized that the template-mediated autocatalysis of POMs provides crucial information in relation to the driving force that directs the assembly of these chemical systems (Figure 1). That is, the formation of discrete products out of a plethora of infinite combinations is only possible due to the selective use of building blocks that can be recognized and take part in the autocatalytic cycle, such as $\{Mo_1\}$, $\{Mo_2\}$, $\{Mo_3\}$, $\{XMo_3\}$, and $\{Mo_6\}$, able to carry specific chemical and structural information. Given the importance of lower nuclearity species, due to their involvement in larger autocatalytic sets and cross-catalyzed systems that produce nanosized high nuclearity molecular metal oxides, we envisaged to investigate and identify the autocatalytic behavior of different species that belong to the Keggin family of molecular metal oxides with the general formula $[XMo_{12}O_{40}]^{x-}$ (X = P, As or Si) – $[AsMo_{12}O_{40}]^{3-}$ and $[SiMo_{12}O_{40}]^{4-}$ (Figure 2).

It is important to note here that in the cases of self-assembled complex multinuclear systems such as the family of POMs, it is not possible to decouple and investigate individually the numerous equilibria established in the reaction mixture, which dynamically alter the presence and the relevant concentrations of the constituents involved. Thus, autocatalytic cycles, self-replication processes, and templated catalytic cycles coexist and feed into one another within the same system. The ability,

however, to determine and monitor over time the presence and concentrations of the species at the beginning of the reaction ($t_o$) and of the final product at the end of the reaction ($t_f$) allows us to observe the overall behavior of the system, identifying conceptually the underlying phenomena and the unique effects that are masked by the vagueness of self-assembly terminology.

Preliminary results indicated previously that the formation of the $\{PMo_{12}\}$ anion is part of an autocatalytic pathway and very fast kinetics. The use of a stopped-flow UV-vis apparatus was necessary in this case to monitor the reaction kinetics which was carried out by mixing freshly prepared solutions of $Na_2MoO_4{\cdot}2H_2O$, and $H_3PO_4/HClO_4$, allowing us to identify the characteristic signature of autocatalytic systems[5] while provided the first hint that autocatalysis might be common and not an artifact among the members of the Keggin family. The obtained information offers a unique opportunity for the exploration of the other members of the Keggin family and allows us to determine if the autocatalytic traits and the fast kinetics are inherent properties of the whole Keggin family.

## RESULTS AND DISCUSSION

Here we discuss our experimental efforts to monitor the formation mechanism of the $\{AsMo_{12}\}$ and $\{SiMo_{12}\}$ species where the use of a conventional UV/Vis detection set up, equipped with a temperature control system, proved to be sufficient. The choice of these Keggin species was based on the size and charge difference of the incorporated $\{XO_4\}^{n-}$ templates and the consistency of the experimental conditions that drives their formation. This allowed a direct comparison to be made and helped us to reach some conclusions in relation to the underlying chemical processes that take place during their formation. The first set of data were obtained for a reduced version of the $[AsMo_{12}O_{40}]^{3-}$ Keggin, where freshly prepared solutions of $Na_2MoO_4{\cdot}2H_2O$, ascorbic acid, and $Na_2HAO_4{\cdot}7H_2O$ were mixed inside a 10-mm cuvette at quantities of 0.5, 1.5, and 2 mL, respectively. The pH value of the reaction mixture at t = 0 falls in the range of 3.6 to 3.8, which are the optimum conditions for the Keggin species formation. The use of reducing agent allowed us to monitor over time the concentration of the final product. In the absence of a reducing agent, the final product exhibits a shoulder in the 200- to 300-nm region of the UV-vis spectrum, where other smaller fragments can contribute making it impossible to monitor unambiguously the formation process of the Keggin species. The reaction was carried out at 5 °C as we recorded in real time the $\lambda_{max}$ of the UV-vis signal centered at 800 nm (Figure 3). Interestingly, the increase of the concentration of the species formed in solution as a function of the time followed a sigmoidal trend, which is indicative of an underlying autocatalytic process.

To investigate further the potential effect of the heteroatom on the catalytic cycle and determine if the autocatalysis is a general property of the Keggin family and not heteroatom specific, we investigated the formation reaction of the reduced $\{SiMo_{12}\}$ Keggin in a similar manner. The same UV/Vis set up was used under the same experimental conditions. This time, freshly prepared solutions of $Na_2MoO_4{\cdot}2H_2O$, ascorbic acid, and $Na_2SiO_3$ were used. Although this reaction was carried out at twice the concentration, the reaction is much slower when compared with the formation of $\{AsMo_{12}\}$ Keggin species.

The characteristic incubation period was detected in a similar fashion, providing evidence that the formation reaction of this system also proceeds via an autocatalytic cycle (Figure 3B).

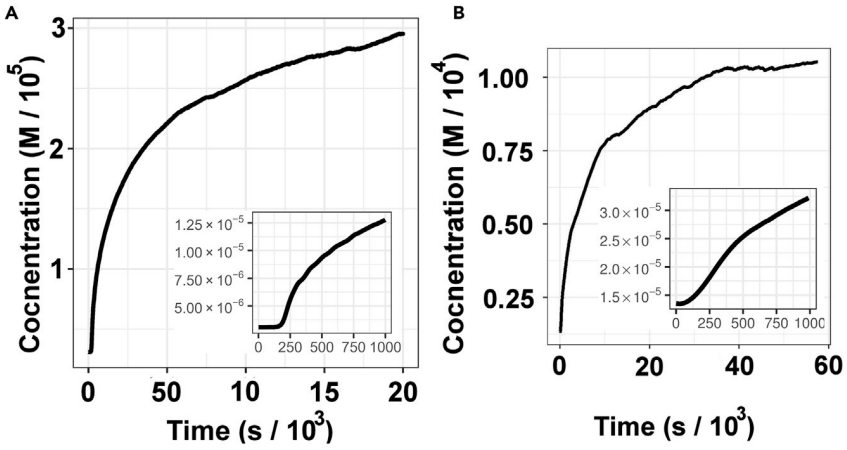


**Figure 3. Concentration-time profiles for {$AsMo_{12}$} and {$SiMo_{12}$}**

(A) Concentration versus time profile of {$AsMo_{12}$} (in $H_2O$ at 5°C), initial concentrations [Mo] = 0.02 M, [$H^+$] = 0.028 M, and [As] = 5 × $10^{-3}$ M. Inset of graph showing lag period at the start of the reaction.

(B) Concentration versus time profile of {$SiMo_{12}$} (in $H_2O$ at 5°C), initial concentrations [Mo] = 0.02M, [$H^+$] = 0.028M, and [Si] = 5 × $10^{-3}$ M. Inset of graphs shows lag period at the start.

To verify further the kinetic behavior of the underlying autocatalytic cycle, we carried out the same reactions using the same stock solutions at various increasing temperatures to test whether they would result in an increase in the rate of the reaction, therefore leading to an increase in the concentration of the species produced as a function of the time. This also allowed us to verify that the presence of the incubation period was not an experimental artifact. Indeed, the temperature increase of the reaction mixture gradually eliminated the lag period that had been observed in the system due to the increased production rate of {$AsMo_{12}$} species, further supporting the hypothesis of an autocatalytic system (Figures 4A and 4B). Since the presence of the incubation period is a necessary but not a sufficient requirement on its own to verify the presence of template autocatalysis, it was envisaged that the autocatalysis occurs via a molecular recognition process where the presence of a species is required to act as a template for the further formation of another cluster in the reaction mixture. A key feature of autocatalytic systems is that, during the initial stages of the reaction, the process occurs primarily via an uncatalyzed pathway, which is the cause of the observed lag time.[31–33] However, once a critical concentration of the catalyst is formed in solution, the explosive growth of the autocatalytic cycle is observable. Therefore, the introduction of presynthesized {$AsMo_{12}$}, at the beginning of the reaction ($t$ = 0), should result in the elimination of the induction period in the rate profile for the reaction and in an increase of the initial rate. To verify our hypothesis, a fixed volume of the preformed {$AsMo_{12}$} solution (0.05 mL) was added at incrementally increasing concentrations to the original mixture and the reaction was followed with UV-vis spectroscopy once more as a function of the time. This presynthesized {$AsMo_{12}$} was made at six different concentrations – 1.19 × $10^{-7}$, 3.83 × $10^{-7}$, 5.73 × $10^{-7}$, 7.65 × $10^{-7}$, 1.16 × $10^{-6}$, and 1.53 × $10^{-6}$ M. The most significant change upon addition of a seed is the gradual elimination of the lag period (Figure 4C), providing further support and reinforcing the hypothesis that the {$AsMo_{12}$} is formed via a template-mediated process whereby the cluster is part of equilibria involved in autocatalytic sets. As shown in Figure 4D, autocatalyst saturation occurs after addition of 1.16 × $10^{-6}$ M of preformed {$AsMo_{12}$}, inducing maximization of the self-propagated rate

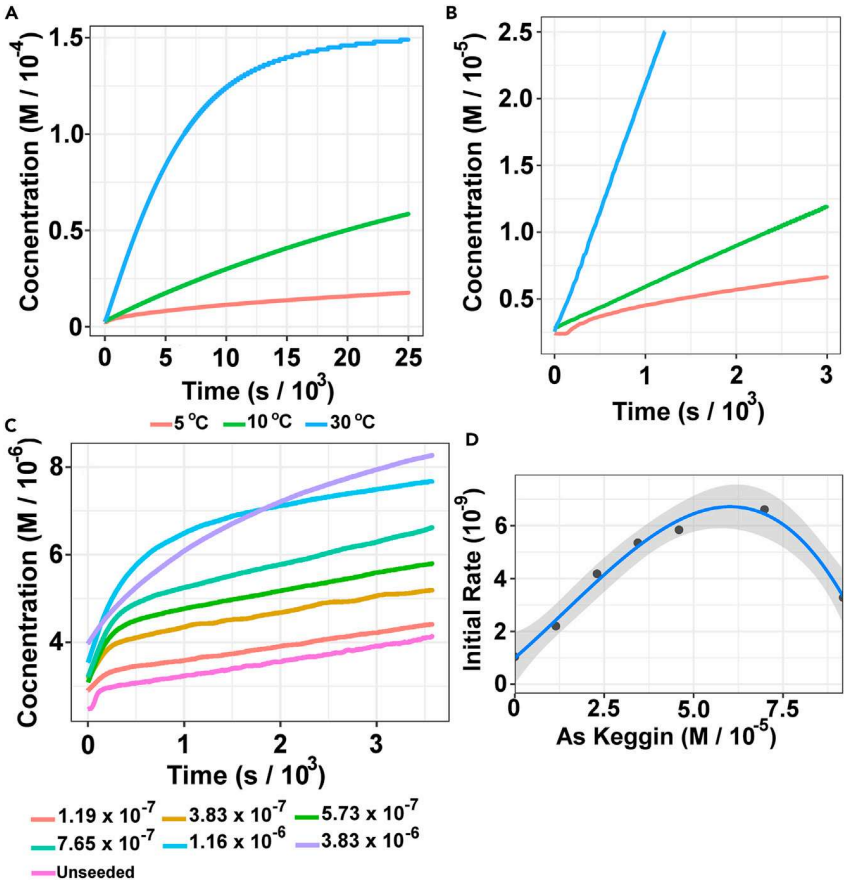


**Figure 4. Concentration-time and saturation plots for {AsMo$_{12}$}**

(A) Concentration versus time profile of {AsMo$_{12}$} $H_2O$, initial concentrations [Mo] = 0.01 M, [$H^+$] = 0.014 M. The data represent the concentration profile versus time of the same reaction at different temperatures.

(B) Inset of graph (A), showing disappearance of lag period upon increased temperature.

(C) Concentration versus time profile of {AsMo$_{12}$} (in $H_2O$ at 5°C), initial concentrations of [Mo] = $4 \times 10^{-3}$ M and [$H^+$] = $5.65 \times 10^{-3}$ M. The data represent the concentration profile versus time of the same reaction mixture seeded with preformed {AsMo$_{12}$} at $1.15 \times 10^{-5}$ M.

(D) Kinetic saturation of {AsMo$_{12}$} autocatalyst. Formation rate versus concentration of {AsMo$_{12}$} injected in the reaction mixture (in $H_2O$ at 5°C). The injected [Mo] concentration of the seed shown in (D) was $1.15 \times 10^{-5}$, $2.3 \times 10^{-5}$, $3.9 \times 10^{-5}$, $4.6 \times 10^{-5}$, $6.9 \times 10^{-5}$ and $8.05 \times 10^{-5}$, respectively. The experimental data points represent the initial rate of the system. An increase is observed at the beginning before reaching a plateau (saturation) where the rate increase by a factor of six before dropping off after the saturation point.

of {AsMo$_{12}$}, as expected. These results encouraged us to further investigate the behavior of the {SiMo$_{12}$} system at various temperatures, in a similar way as described previously for the {AsMo$_{12}$}, and more specifically on the incubation period. Indeed, the temperature increase led to the gradual elimination of the incubation period due to the increased production rate of the {SiMo$_{12}$} Keggin species (Figures S1 and S2).

Finally, the additional verification of the presence of autocatalytic cycle in the system involved the seeding of the reaction mixture with preformed {SiMo$_{12}$}, much like the {AsMo$_{12}$}, but at an increased concentration and volume. This presynthesized {SiMo$_{12}$} was then made up to five different solution concentrations – $4.78 \times 10^{-7}$,

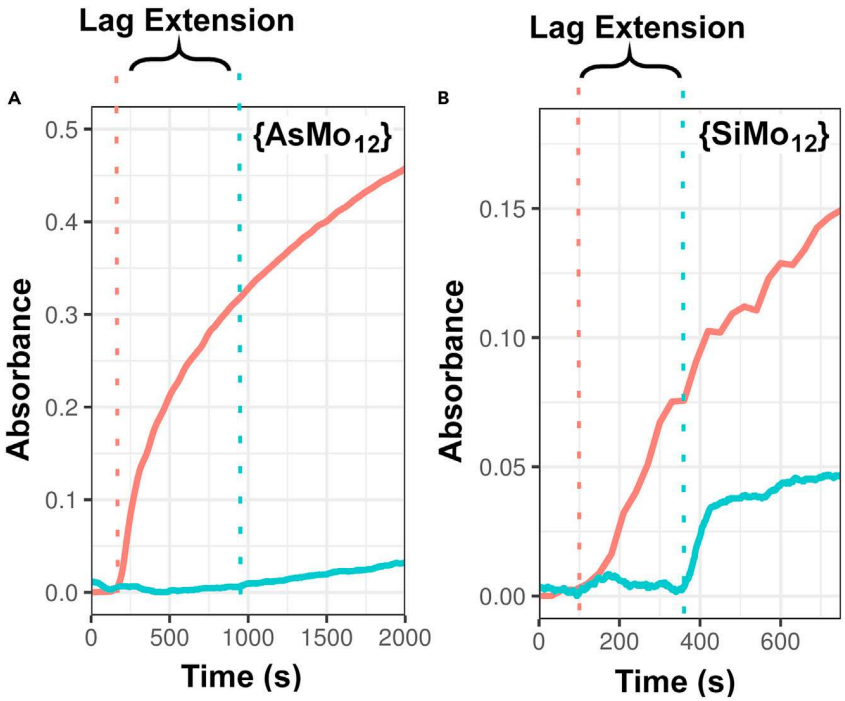


**Figure 5. Concentration-incubation period effects for $\{AsMo_{12}\}$ and $\{SiMo_{12}\}$**

(A and B) Representation of the effect of the [Mo] on the induction period for: (A) $\{AsMo_{12}\}$ and (B) $\{SiMo_{12}\}$, respectively. Color code: light blue, [Mo] = $3 \times 10^{-4}$; light red, [Mo] = $3 \times 10^{-3}$.

$9.12 \times 10^{-7}$, $1.92 \times 10^{-6}$, $2.87 \times 10^{-6}$, and $3.83 \times 10^{-6}$ M. Again, the reaction inside the cuvette remained the same but 0.05 mL additions of the seed were injected at the incrementally increased concentrations. Upon addition of the preformed $\{SiMo_{12}\}$, an increased formation rate was observed at the beginning of the reaction, leading to the elimination of the lag period (Figure S3A) and kinetic saturation of the system upon addition of $9.12 \times 10^{-7}$ M of preformed $\{SiMo_{12}\}$ (Figure S3B) providing further support that this member of Keggin species also catalyzes its own formation via a template-mediated process.

Additionally, we embarked on exploring further the incubation periods observed during the formation of the Keggin species. More specifically, we explored the effect of the concentration on the length of the observed lag. More specifically, the lag time has increased from 180 to 900 s in the case of $\{AsMo_{12}\}$ and from 130 to 380 s in the case of $\{SiMo_{12}\}$ by reducing the initial concentrations of molybdenum by an order of magnitude according to Figure 5.

Based on the above observations, it is quite intriguing that all members of the Keggin family exhibit autocatalytic traits. However, the autocatalytic behavior is markedly different. This is potentially due to the interplay between the size and overall negative charge of the $\{XO_4\}$ (X = P, Si, As) anionic templates. The bigger size and larger overall negative charge of the $\{XO_4\}$ template, seems to slow down the autocatalytic cycle. It is interesting that autocatalytic processes constitute a favorable resource for the formation of smaller nuclearity molecular metal oxides as well, and its manifestation does not depend on the type of the heteroatom. However, the rate of the autocatalytic cycle can be manipulated and is directly related to the size and charge of the heteroatom.

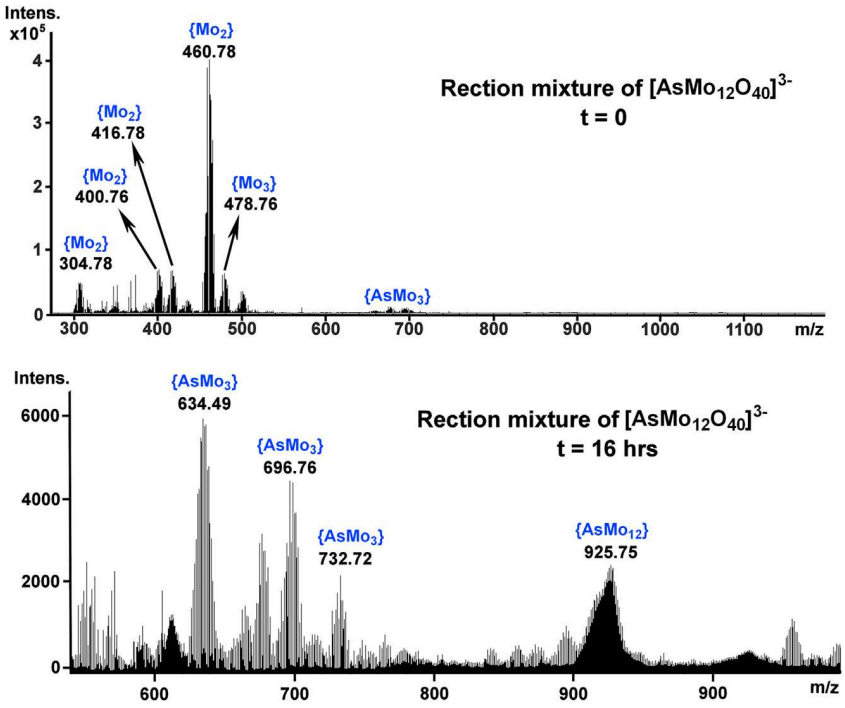


**Figure 6. Negative mode electrospray ionization mass spectrum (ESI-MS) of the {$AsMo_{12}$} reaction mixture in $H_2O$ at t = 0 h (top) and t = 16 h (bottom)**
See also Figures S4–S8.

## Real-time monitoring of reaction mixture by ESI-MS

After establishing evidence to support a template autocatalytic reaction mechanism driving the formation of the Keggin species, we sought to refine the mechanistic steps in the process. A key point required clarification in our effort to shed light on the formation mechanism of the Keggin family members, was the identification of species that are involved in the detected autocatalytic set. To explore this, we used electrospray ionization mass spectrometry (ESI-MS) and detected the species that are present in the reaction mixture upon mixing of the starting materials (t = 0) and after 16 h (Figure 6). Interestingly, at t = 0 the only species that are detectable were singly charged {$Mo_2$} units such as $[Mo_2O_7H]^-$, $[Mo_2O_7Na(H_2O)_4]^-$, $[Mo_2O_7Na(H_2O)_5]^-$ and $[Mo_2^{VI}O_9Na_3(H_2O)_3H_2]^-$ centered at 304.78, 400.76, 416.78 and 460.78 m/z, singly charged {$Mo_3$} unit, $[Mo^{V}Mo_2^{IV}O_9Na_2H_2]^-$ centered at 478.76 m/z and amounts of {$AsMo_3$} units such as $[Mo_3^{VI}O_9(AsO_4)Na_2(H_2O)]^-$, $[Mo_3^{VI}O_{10}(AsO_4)Na_4(H_2O)]^-$ and $[Mo_3^{VI}O_{10}(AsO_4)Na_4(H_2O_3)]^-$ centered at 634.49, 696.76, and 732.60 m/z, respectively. After 16 h, solution studies revealed the presence of {$AsMo_3$} units such as $[Mo_3^{VI}O_9(AsO_4)H_2]^-$, $[Mo_3^{VI}O_9(AsO_4)NaH]^-$, $[Mo_3^{VI}O_9(AsO_4)Na_2(H_2O)]^-$, $[Mo_3^{VI}O_{10}(AsO_4)Na_4]^-$, $[Mo_3^{VI}O_{10}(AsO_4)Na_4(H_2O)]^-$, $[Mo_3^{VI}O_{10}(AsO_4)Na_4(H_2O)_2]^-$, and $[Mo_3^{VI}O_{10}(AsO_4)Na_4(H_2O)_3]^-$ centered at 572.61, 594.58, 634.49, 678.60, 696.76, 716.59, and 732.60 m/z and the doubly charged $[AsMo_{11}^{VI}Mo^{V}O_{39}H]^{2-}$ Keggin anion centered at 925.75 m/z value (see also Figures S4–S8). These results suggest that not only do the {$Mo_2$} and {$Mo_3$} units form rapidly in solution, but also show that building blocks of other sizes did not form at comparable concentrations. These observations informed the construction of the kinetic model described below. It is important to note here that the ESI-MS solution studies are extremely useful in revealing information about the stability or the presence of species in the reaction mixture or exclude the presence of other

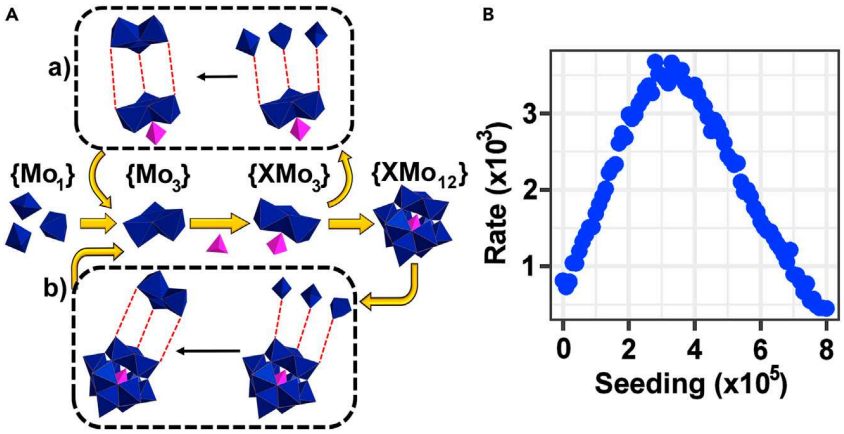


**Figure 7. Proposed autocatalytic cycles and stochastic model**

(A) Hypothesized embedded autocatalytic cycles. (a) The final {$XMo_{12}$} Keggin product and the {$XMo_3$} subunit are responsible for the templating of more {$Mo_3$} building blocks. (b) The subsequent templating of more {$Mo_3$} subunits allow for an exponential production of the {$XMo_{12}$} Keggin.

(B) A dynamic model of the reaction pathway hypothesized in Figure 7A is consistent with the observed kinetic saturation. Details of the model can be found in the supplemental information. See also Figures S9 and S10.

POM species that might form in solution but cannot determine the concentration of the individual species, which would allow us to study individually the different equilibria that coexist in solution.

## Modeling of the reaction pathway

A consistent feature of the dynamics observed here, for all the {$PMo_{12}$}, {$AsMo_{12}$}, and {$SiMo_{12}$} clusters is the observation of kinetic saturation of the initial rate upon seeding, which is shown for the {$AsMo_{12}$} in Figure 4D. To better understand the dynamics behind this phenomenon, we implemented a computational model of the proposed reaction pathway based on the evidence provided by the conducted solution studies using temperature-controlled UV-vis and ESI-MS at different time intervals. Briefly, in this model all reactions proceed as either bimolecular or unimolecular reactions. This indicates that the formation of the {$Mo_3$} building block from molybdate occurs in two steps with an {$Mo_2$} intermediate, which can degrade back into molybdate or further reactions with other molybdate to form {$Mo_3$}. We model the template catalysis of species by including a reaction where a molybdate can first attach to the template surface and then proceed to add more molybdate in a stepwise fashion, each step of which is reversible. We included both {$XMo_3$} and {$XMo_{12}$} as templates for the formation of {$Mo_3$}, as hypothesized in Figure 7A. This is because, based on the experimental evidence collected, these compounds are produced in abundance, while other species are not. To explain the autocatalytic properties observed, some of these species must be involved in the process. Using this model, we explored the effect of increasing the initial amount of {$XMo_{12}$}, and the results are shown in Figure 7B (See also Figures S9 and S10).

The model is consistent with the kinetic saturation seen in the physical experiments and can be explained by the template mechanism.[36,37] When the initial amount of the template is low relative to the amount of molybdate, templates accelerate the formation of {$Mo_3$}, which then reacts to form more of the {$XMo_{12}$} template and adding more {$XMo_3$} increases this rate. This is true until the number of template surfaces

becomes too large for the initial amount of molybdate. At that point, individual molybdates attach to templates but are unlikely to react with other molybdates (because they are themselves attached to templates), this means the net formation of the $\{XMo_{12}\}$ is reduced because of the time required for the unreacted molybdate to dissociate from the template and react with other template complexes. The fact that both the $\{XMo_3\}$ and $\{XMo_{12}\}$ can serve as templates by bringing together 3 × $\{Mo_1\}$ to form additional $\{Mo_3\}$ building blocks and finally Keggin species, means that the amount of $\{XMo_{12}\}$ at which this happens is much lower than the initial amount of molybdate.

In conclusion, we identified the presence of autocatalytic traits in the formation of the Keggin family of POM species such as $\{AsMo_{12}\}$ and $\{SiMo_{12}\}$. Real-time monitoring UV/Vis studies have shown that the formation of Keggin species proceeds via a templated autocatalytic mechanism exhibiting an early uncatalyzed stage leading to an incubation period of approximately 200 s as well as kinetic saturation effects in the presence of a preformed catalyst, confirming the presence of an embedded autocatalytic cycle and an underlying molecular template process. Another interesting observation is the influence of the heteroatom on the autocatalytic cycle of the Keggin species. More specifically, there is an interplay between the ionic radius and the overall charge on the $\{XO_4\}^{n-}$ central component and the operational rate of the autocatalytic cycle. The higher overall charge and smaller ionic radius seems to be beneficial for the operation rate of the autocatalytic cycle. The $\{As^{V}O_4\}^{3-}$ templated Keggin appears to form at faster rates than the $\{Si^{IV}O_4\}^{4-}$ templated one, even though the As-heteroatom exhibits larger ionic radius if compared with the $Si^{IV}$. In the case of $\{P^{V}O_4\}^{3-}$ (reported previously), which carries the same charge but with a smaller radius than the $\{As^{V}O_4\}^{3-}$, appears to be considerably faster among the investigated $\{XO_4\}^{n-}$ templated species. Finally, the unveiled knowledge and embedded processes within this family of inorganic clusters, provides crucial evidence for the deeper understanding of the underlying chemical processes usually vaguely described as self-assembly. Most important, this observation not only contributes to the better understanding of the masked chemical processes, but also can be extrapolated and used constructively for the discovery of new forms of materials. The underlying processes can now be manipulated at the molecular level and be used as functional modules leading to the design of extended and interactive chemical operations where the outcome is determined by the combination of the modules used.

## EXPERIMENTAL PROCEDURES

### Resource availability

#### *Lead contact*

Further information and requests for resources and materials should be directed to and will be fulfilled by the lead contact, Leroy Cronin (lee.cronin@glasgow.ac.uk).

#### *Materials availability*

This study did not generate new unique reagents.

#### *Data and code availability*

The published article includes all data analyzed during this study.

## SUPPLEMENTAL INFORMATION

Supplemental information can be found online at https://doi.org/10.1016/j.matt.2021.11.030.

## ACKNOWLEDGMENTS

We gratefully acknowledge financial support from the EPSRC grants (No. EP/J015156/1; EP/L023652/1; EP/I033459/1; EP/K023004/1). L.C. thanks the ERC for an Advanced Grant (ERC-ADG, 670467 SMART-POM).

## AUTHOR CONTRIBUTIONS

The idea was conceived by L.C. and H.M. D.L. carried out the reactions and analyzed the data with help from H.M. C.M. developed the model. All the authors helped to write the manuscript.

## DECLARATION OF INTERESTS

The authors declare no competing interests.

Received: July 26, 2021
Revised: November 20, 2021
Accepted: November 26, 2021
Published: December 17, 2021

## REFERENCES

1. Miras, H.N., Yan, J., Long, D.-L., and Cronin, L. (2012). Engineering polyoxometalates with emergent properties. Chem. Soc. Rev. *41*, 7403–7430.

2. Schäffer, C., Todea, A.M., Bögge, H., Cadot, E., Gouzerh, P., Kopilevich, S., Weinstock, I.A., and Müller, A. (2011). Softening of pore and interior properties of a metal-oxide-based capsule: substituting 60 oxide by 60 sulfide ligands. Angew. Chem. Ed. Int. *50*, 12326–12329.

3. Zang, H.Y., Purcell, J.W., Long, D.L., Miras, H.N., and Cronin, L. (2017). Exploring structural complexity in the discovery and self-assembly of a family of nanoscale chalcoxides from $\{Se_8Mo_{36}\}$ to $\{Se_{26}Mo_{68}\}$. Chem. Commun. *53*, 8585–8587.

4. Miras, H.N., Vilà-Nadal, L., and Cronin, L. (2014). Polyoxometalate based open-frameworks (POM-OFs). Chem. Soc. Rev. *43*, 5679–5699.

5. Miras, H.N., Mathis, C., Xuan, W., Long, D.L., Pow, R., and Cronin, L. (2020). Spontaneous formation of autocatalytic sets with self-replicating inorganic metal oxide clusters. Proc. Natl. Acad. Sci. U S A *117*, 10699–10705.

6. Craig, L.H., and Goodrich, C.W. (1998). Introduction: polyoxometalatessMulticomponent molecular vehicles to probe fundamental issues and practical problems. Chem. Rev. *98*, 1–2.

7. Keggin, J.F. (1933). Structure of the molecule of 12-phosphotungstic acid [2]. Nature *131*, 908–909.

8. Al-Oweini, R., Bassil, B.S., Itani, M., Emiroğlu, D.B., and Kortz, U. (2018). The mixed-valent 10-manganese(III/IV)-containing 36-tungsto-4-arsenate(V), $[Mn^{III}_6Mn^{IV}_4O_4(OH)_{12}(H_2O)_{12}(A\text{-}\beta\text{-}AsW_9O_{34})_4]^{22-}$. Acta Crystallogr. Sect. C *74*, 1390–1394.

9. Barsukova-Stuckart, M., Izarova, N.V., Barrett, R., Wang, Z., van Tol, J., Kroto, H.W., Dalal, N.S., Keita, B., Heller, D., and Kortz, U. (2012). 3D metal ions in highly unusual eight-coordination: the phosphate-capped dodecapalladate(II) nanocube. Chem. A. Eur. J. *18*, 6167–6171.

10. Al-Oweini, R., Sartorel, A., Bassil, B.S., Natali, M., Berardi, S., Scandola, F., Kortz, U., and Bonchio, M. (2014). Photocatalytic water oxidation by a mixed-valent $Mn^{III}_3Mn^{IV}O_3$ manganese oxo core that mimics the natural oxygen-evolving center. Angew. Chem. Int. Ed. *53*, 11182–11185.

11. Mitchell, S.G., Molina, P.I., Khanra, S., Miras, H.N., Prescimone, A., Cooper, G.J.T., Winter, R.S., Brechin, E.K., Long, D.L., Cogdell, R.J., et al. (2011). A mixed-valence manganese cubane trapped by inequivalent trilacunary polyoxometalate ligands. Angew. Chem. Int. Ed. *50*, 9154–9157.

12. Molina, P.I., Miras, H.N., Long, D.-L., and Cronin, L. (2014). Assembly and core transformation properties of two tetrahedral clusters: $[Fe^{III}_{13}P_8W_{60}O_{227}(OH)_{15}(H_2O)_2]^{30-}$ and $[Fe^{III}_{13}P_8W_{60}O_{224}(OH)_{12}(PO_4)_4]^{33-}$. Dalton Trans. *43*, 5190–5199.

13. Long, D.L., Tsunashima, R., and Cronin, L. (2010). Polyoxometalates: building blocks for functional nanoscale systems. Angew. Chem. Int. Ed. *49*, 1736–1758.

14. Cameron, J.M., Vilà-Nadal, L., Winter, R.S., Iijima, F., Murillo, J.C., Rodríguez-Fortea, A., Oshio, H., Poblet, J.M., and Cronin, L. (2016). Investigating the transformations of polyoxoanions using mass spectrometry and molecular dynamics. J. Am. Chem. Soc. *138*, 8765–8773.

15. Miras, H.N., Wilson, E.F., and Cronin, L. (2009). Unravelling the complexities of inorganic and supramolecular self-assembly in solution with electrospray and cryospray mass spectrometry. Chem. Commun. *11*, 1297–1311.

16. Deery, M.J., Howarth, O.W., and Jennings, K.R. (1997). Application of electrospray ionisation mass spectrometry to the study of dilute aqueous oligomeric anions and their reactions. J. Chem. Soc. Dalton Trans. *24*, 4783–4788.

17. Ohlin, C.A. (2012). Reaction dynamics and solution chemistry of polyoxometalates by electrospray ionization mass spectrometry. Chem. Asian J. *7*, 262–270.

18. Vilà-Nadal, L., Wilson, E.F., Miras, H.N., Rodríguez-Fortea, A., Cronin, L., and Poblet, J.M. (2011). Combined theoretical and mass spectrometry study of the formation-fragmentation of small polyoxomolybdates. Inorg. Chem. *50*, 7811–7819.

19. Nakamura, I., Miras, H.N., Fujiwara, A., Fujibayashi, M., Song, Y.F., Cronin, L., and Tsunashima, R. (2015). Investigating the formation of "molybdenum blues" with gel electrophoresis and mass spectrometry. J. Am. Chem. Soc. *137*, 6524–6530.

20. Xu, F., Scullion, R.A., Yan, J., Miras, H.N., Busche, C., Scandurra, A., Pignataro, B., Long, D.L., and Cronin, L. (2011). A supramolecular heteropolyoxopalladate {Pd15} cluster host encapsulating a $\{Pd_2\}$ dinuclear guest: $[Pd^{II}_2\subset\{H_7Pd^{II}_{15}O_{10}(PO_4)_{10}\}]^{7-}$. J. Am. Chem. Soc. *133*, 4684–4686.

21. Miras, H.N., Zang, H.Y., Long, D.L., and Cronin, L. (2011). Direct synthesis and mass spectroscopic observation of the {M40} polyoxothiometalate wheel. Eur. J. Inorg. Chem. 5105–5111. https://doi.org/10.1002/ejic.201100833.

22. Nadal, L.V., Rodríguez-Fortea, A., Yan, L.K., Wilson, E.F., Cronin, L., and Poblet, J.M. (2009). Nucleation mechanisms of molecular oxides: a study of the assembly-dissassembly of $[W_6O_{19}]^{2-}$ by theory and mass spectrometry. Angew. Chem. Int. Ed. *48*, 5452–5456.

23. Schreiber, R.E., Houben, L., Wolf, S.G., Leitus, G., Lang, Z.L., Carbó, J.J., Poblet, J.M., and Neumann, R. (2017). Real-time molecular scale

observation of crystal formation. Nat. Chem. *9*, 369–373.

24. López, X., Carbó, J.J., Bo, C., and Poblet, J.M. (2012). Structure, properties and reactivity of polyoxometalates: a theoretical perspective. Chem. Soc. Rev. *41*, 7537–7571.

25. Sures, D., Segado, M., Bo, C., and Nyman, M. (2018). Alkali-driven disassembly and reassembly of molecular niobium oxide in water. J. Am. Chem. Soc. *140*, 10803–10813.

26. Nghe, P., Hordijk, W., Kauffman, S.A., Walker, S.I., Schmidt, F.J., Kemble, H., Yeates, J.A.M., and Lehman, N. (2015). Prebiotic network evolution: six key parameters. Mol. Biosyst. *11*, 3206–3217.

27. Kauffman, S.A. (1986). Autocatalytic sets of proteins. J. Theor. Biol. *119*, 1–24.

28. Hordijk, W., and Steel, M. (2012). Autocatalytic sets extended: dynamics, inhibition, and a generalization. J. Syst. Chem. *3*, 5.

29. Sievers, D., and von Kiedrowski, G. (1994). Self-replication of complementary nucleotide-based oligomers. Nature *369*, 221–224.

30. Lee, D.H., Granja, J.R., Martinez, J.A., Severin, K., and Ghadiri, M.R. (1996). A self-replicating peptide. Nature *382*, 525–528.

31. Kassianidis, E., and Philp, D. (2006). Design and implementation of a highly selective minimal self-replicating system. Angew. Chem. Int. Ed. *45*, 6344–6348.

32. Sadownik, J.W., and Philp, D. (2008). A simple synthetic replicator amplifies itself from a dynamic reagent pool. Angew. Chem. Int. Ed. *47*, 9965–9970.

33. Quayle, J.M., Slawin, A.M.Z., and Philp, D. (2002). A structurally simple minimal self-replicating system. Tetrahedron Lett. *43*, 7229–7233.

34. Vidonne, A., and Philp, D. (2009). Making molecules make themselves - the chemistry of artificial replicators. Eur. J. Org. Chem. *5*, 593–610.

35. Bissette, A.J., and Fletcher, S.P. (2013). Mechanisms of autocatalysis. Angew. Chem. Int. Ed. *52*, 12800–12826.

36. Haruna, I., and Spiegelman, S. (1965). Autocatalytic synthesis of a viral RNA in vitro. Science *150*, 884–886.

37. Schuster, P. (2019). What is special about autocatalysis? Monatsh. Chem. *150*, 763–775.